A Coupled-Inductor-Based Soft-Switching Non-Inverting Buck-Boost Converter with Reduced Auxiliary Component Count

Guo Xu, *Member*, *IEEE*, Kang Hong, Guangfu Ning, *Member*, *IEEE*, Wenjing Xiong, *Member*, *IEEE*, Yao Sun, *Member*, *IEEE*, and Mei Su, *Member*, *IEEE*

***Abstract*—This paper proposes a coupled-inductor-based soft switching non-inverting Buck-Boost Converter (NIBBC) with reduced auxiliary component count. Instead of using multiple auxiliary passive components to achieve soft switching, the proposed coupled-inductor-based NIBBC uses the coupled inductor as the main inductor, and the auxiliary current generated by the magnetic coupling effect is used to obtain the soft switching for all switches. With simple PWM modulation under fixed frequency, full load range ZVS can be obtained under wide voltage range. Unlike the conventional method utilizing the coupled inductor only to generate non-active power, the coupled inductor of the proposed converter also takes participant in the power transmission. Besides, the added diode can achieve zero current turn-off which avoids the diode recovery issue. The operating principle, the soft switching and parameter designs are analyzed in this paper. Finally, experimental results have verified the effectiveness of the proposed solution.**

***Index Terms*— Coupled inductor, non-inverting buck-boost converter, full load range ZVS.**

I. Introduction

Due to its simple structure and wide voltage range conversion capability, the non-inverting buck-boost converters (NIBBC) have been widely used in renewable energy development, energy storage equipment, and even the integration of basic power converter modules as DC distributed power systems in recent years [1], [2]. In order to simplify the control of NIBBC, two switches are often switched synchronously, and so are the other two switches [3], [4]. In that case, NIBBC has two control variables, which include two duty cycles for the two sets of switches. Such control is easy for implementation, but because there are always two switches working under hard-switching [5], the converter efficiency is reduced [6]. In order to reduce the switching loss, the zero-voltage switching (ZVS) technology of NIBBC has been extensively studied [7]-[16]. According to the types of auxiliary devices, these methods can be roughly divided into two categories: none auxiliary circuit and auxiliary circuit.

The none auxiliary circuit NIBBC mostly uses triangular current mode (TCM) operation and corresponding modulation method to provide soft switching conditions for NIBBC without adding redundant auxiliary equipment [9]. However, the frequency is changeable, and the propagation delay and dead time of the comparator will cause unpredictable output voltage ripple, which will cause the converter to malfunction. Ripple interference can be eliminated by a mode conversion technique controlled by duty cycle lock [10]. The controller proposed in [11] can eliminate the ripple interference while keeping other system parameters within an acceptable range. However, the control complexity of the converter is increased.

In order to realize all the soft-switching conditions of NIBBC and simplify the control strategy, auxiliary circuits can be added. Reference [12] uses an auxiliary circuit composed of an inductor, an auxiliary switch and a power diode to realize ZVS. Although the volume of the auxiliary circuit is reduced, additional control method and driver circuit are needed. Reference [13] proposes ZVS NIBBC using LC circuit. The proposed converter can realize ZVS at different load currents by using current cycling of auxiliary inductors and capacitors. References [14]-[16] propose a coupled inductor auxiliary circuit, which uses the magnetic coupling effect to generate auxiliary current to achieve ZVS, and the soft switching range can be adjusted by adjusting the auxiliary current. However, in [14]-[16], the coupled inductor is used as auxiliary circuit to provide the circulating current to help achieve ZVS, which does not contribute to the output power, and could increase the related losses. In addition, at least five auxiliary components are added for these solutions.

In addition, switched resonator DC/DC converter with a single switch and small inductors could enhance the power density, but the ZVS range is narrow and the design is complex [17]. In most cases, high-performance resonant converter control requires a continuous adaptation of the power device switching instances depending on the power input source, load

Manuscript received December 16, 2020; revised March 13, 2021; accepted June 18, 2021. This work was supported in part by the Nature Science Foundation of China under Grant 51907206 and 61933011, the Hunan Provincial Key Laboratory of Power Electronics Equipment and Grid under Grant 2018TP1001, in part by the Major Project of Changzhutan Self-dependent Innovation Demonstration Area under Grant 2018XK2002. (Corresponding author: Guangfu Ning).

G. Xu, K. Hong, G. Ning, W. Xiong, Y. Sun and M. Su are with the School of Automation, Central South University and with Hunan Provincial Key Laboratory of Power Electronics Equipment and Grid, Changsha, 410083, China, (e-mail: xuguocsu@csu.edu.cn; hong kang@csu.edu.cn; ningguangfu@csu.edu.cn; xiongwj@csu.edu.cn; yaosuncsu@gmail.com; sumeicsu@mail.csu.edu.cn).

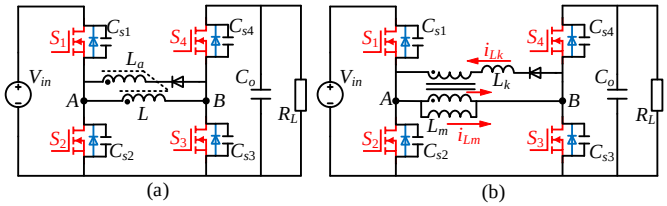

Fig. 1. Proposed NIBBC. (a) Circuit topology. (b) Equivalent circuit.

current, or parameter variation in passive components. If the resonant converter is switched before or after the resonant swing ends, it will suffer from higher losses [18]. In addition, for high power applications, the inrush current during start-up needs to be specially dealt with. The bridge structure is adopted in proposed NIBBC because of low voltage stress, wide voltage range and simple structure, which is widely studied and used in the industrial applications [19]-[20] and is also the focus of this paper.

To achieve soft switching with fewer auxiliary components, a new coupled-inductor-based soft-switching NIBBC is proposed in this paper. Compared with other methods in [12]-[16], the proposed soft-switching NIBBC has the fewest auxiliary components. It only utilizes coupled inductor and one diode to achieve full load range ZVS under wide voltage range. Besides, unlike the conventional method utilizing the coupled inductor only generating non-active power, the coupled inductor of the proposed converter also takes participant in the power transmission.

II. Topology and Working Principle

A. Proposed Topology

The proposed NIBBC structure and equivalent circuit are shown in Fig. 1. C_{sn} ($n = 1-4$) is the junction capacitor of switch S_n; C_o is the output filter capacitor; L is the main inductor; L_a is the auxiliary inductor (L is coupled with L_a). L_m and L_k are the equivalent inductance after adopting the cantilever model, i_{Lm} and i_{Lk} are the currents flowing through the two inductors respectively (the reference direction is shown in Fig. 1(b)), and V_{in} is the DC voltage source. k is the coupling coefficient. If $-1<k<1$, a negative value represents reverse coupling, and a positive value represents positive coupling. Compared with the NIBBC in [16], at least one inductor and two capacitors can be removed, which could reduce the magnetic loss and converter volume.

B. Working Principle

The waveforms of the proposed NIBBC are shown in Fig.2. Since all of the four switches are active switches, and the driving signal for each bridge is complementary, the converter will only operate in CCM mode. The working modes of the proposed NIBBC can be divided into six intervals. Fig. 3 shows the corresponding converter operation mode for each interval.

***Interval* 1 (t_0-t_1):** When S_1 and S_3 are turned off, this interval starts. In this interval, the switch junction capacitors (C_{s1}, C_{s2}, C_{s3}, and C_{s4}) are charging and discharging.

***Interval* 2 (t_1-t_2):** The interval starts when the body diodes of S_2 and S_4 are turned on. In this interval, the drain-source

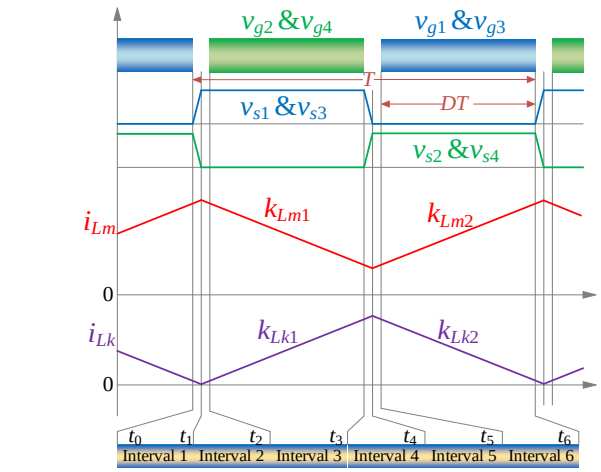

Fig. 2. Waveforms of the proposed NIBBC.

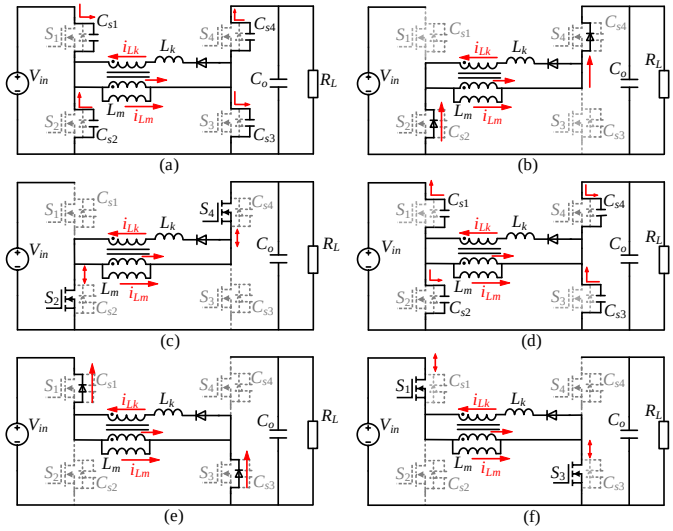

Fig. 3. Six intervals of the proposed NIBBC. (a) Interval 1. (b) Interval 2. (c) Interval 3. (d) Interval 4. (e) Interval 5. (f) Interval 6.

voltages (v_{s2} and v_{s4}) of S_2 and S_4 are reduced to zero, which ensures the zero-voltage turn-on.

***Interval* 3 (t_2-t_3):** This interval starts when S_2 and S_4 are turned on under ZVS conditions. The power is transferred to the output through the coupled inductor.

During this interval, the following equations can be obtained:

$$\begin{cases} V_{Lm} = L_m \dfrac{di_{Lm}}{dt} = -V_o \\ \dfrac{1}{n}V_o - L_k \dfrac{di_{Lk}}{dt} = -V_o \end{cases} \tag{1}$$

where V_o is output voltage, n is the equivalent turns ratio of the coupled inductance cantilever model. These current differential equations will be

$$\begin{cases} k_{Lm1} = \dfrac{di_{Lm}}{dt} = \dfrac{-V_o}{L_m} \\ k_{La1} = \dfrac{di_{La}}{dt} = \dfrac{V_o}{L_k} \cdot \dfrac{n-1}{n} \end{cases}. \tag{2}$$

***Interval* 4 (t_3-t_4):** In this interval, all the switches are off.

***Interval* 5 (t_4-t_5):** At time t_4, the body diodes of S_1 and S_3 are turned on, and then the drain-source voltages (v_{s1} and v_{s3}) of S_1 and S_3 decrease to zero.

***Interval* 6 (t_5-t_6):** Similar to interval 3, at time t_5, S_1 and S_3 are turned on under ZVS conditions. In this interval, power is stored in the couple inductor.

The following equation can be obtained during this interval:

$$\begin{cases} V_{Lm} = L_m \dfrac{di_{Lm}}{dt} = V_{in} \\ \dfrac{1}{n} V_o - L_k \dfrac{di_{Lk}}{dt} = V_{in} \end{cases}. \tag{3}$$

D is the duty cycle of S_1 and S_3, the relationship of V_{in} and V_o can be obtained as

$$V_o = \frac{D}{1-D} V_{in}. \tag{4}$$

And the following equation can be obtained:

$$\begin{cases} k_{Lm2} = \dfrac{di_{Lm}}{dt} = \dfrac{V_o}{L_m} \cdot \dfrac{1-D}{D} \\ k_{La2} = \dfrac{di_{La}}{dt} = \dfrac{-V_o}{L_k} \cdot \dfrac{n-1}{n} \cdot \dfrac{1-D}{D} \end{cases}. \tag{5}$$

III. ZVS Analysis and Design

A. ZVS Analysis

At t_2, the current $i_{Lm}(t_2)$ flowing through L_m is always positive (the direction in Fig. 3(b) is positive), so before S_2 and S_4 are turned on, the direction of the current flowing through is consistent with the direction of the switch body diode. Therefore, S_2 and S_4 of the converter can naturally achieve ZVS. In order to achieve the ZVS conditions of S_1 and S_3, the current at t_5 must satisfy

$$i_{on} = i_{Lk}(t_5) - i_{Lm}(t_5) - \frac{1}{n} i_{Lk}(t_5) > 0 \tag{6}$$

where i_{on} is the turn on current of S_1 and S_3. In steady state operation, the average current I_{Lm} and I_{Lk} can be expressed as

$$I_{Lm} - I_{Lk} + \frac{1}{n} I_{Lk} = \frac{I_o}{1-D} = \frac{P_o}{V_o(1-D)} \tag{7}$$

where I_o is the average current of the load, P_o is the output power. Then $i_{Lk}(t_5)$ and $i_{Lm}(t_5)$ can be expressed as

$$\begin{cases} i_{Lk}(t_5) = \dfrac{V_o T_s (1-D)(n-1)}{n L_k} \\ i_{Lm}(t_5) = \dfrac{V_o T_s (1-D)\left[(n-1)L_m - nL_k\right]}{2nL_m L_k} + \dfrac{P_o}{V_o(1-D)} \end{cases} \tag{8}$$

where T_s is switching period. Substituting (8) to (6), then

$$i_{on} = \frac{V_o T_s (1-D)\left[(n-1)^2 L_m + n^2 L_k\right]}{2n^2 L_m L_k} - \frac{P_o}{V_o(1-D)} > 0. \tag{9}$$

According to the cantilever model, (9) can be transformed into the following relationship:

$$i_{on} = \frac{V_o T_s (1-D)(L + L_a - 2k\sqrt{LL_a})}{2LL_a(1-k^2)} - \frac{P_o}{V_o(1-D)} > 0. \tag{10}$$

The soft-switching condition of the proposed NIBBC is expressed in (10). In order to realize the ZVS, the i_{on} value must be positive. The soft-switching range is related to V_o, P_o, k, D, L, L_a, and T_s.

B. Parameter Design

The parameters with V_{in} = 67-150 V, V_o = 100 V, switching frequency f_s = 100 kHz and P_o = 500 W, are selected as the application background to analyze the effect of k and L on the soft-switching range. When the input voltage is lower than the output voltage (such as: V_{in}=67V, V_o=100V), the converter works in boost mode, on the contrary (such as: V_{in} = 150V, V_o = 100V) it works in buck mode. Due to the existence of diodes in the proposed converter, power can only be transmitted in the forward direction. Therefore, both boost mode and buck mode represent forward power transmission. According to (5), the variation range of D is 0.4-0.6. Since ZVS achievement will become worse if duty cycle increases, V_{in} = 67 V (D = 0.6) is analyzed here. In order to simplify the calculation and the design of the coupled inductor, set the self-inductance of the two coupled inductors to be equal. Then get the mapping of k, L and i_{on}, as shown in Fig. 4(a). A positive value indicates that S_1, S_3 will obtain a soft switching condition, and a negative value indicates that there is no soft-switching condition in this area.

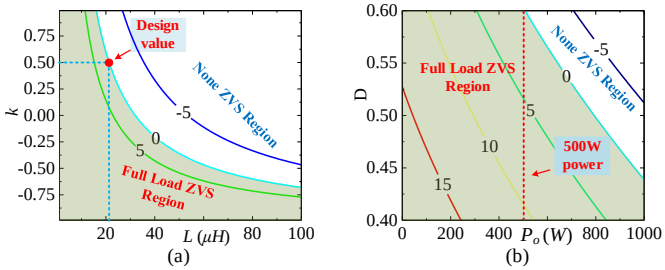

Fig. 4. ZVS Range plots. (a) ZVS range versus L and k with D = 0.6. (b) ZVS range versus P and D with L = 21 μH and k = 0.5.

As the value of i_{on} increases, the current stress of the device will increase. Therefore, in the case of reaching the ZVS condition, hardware parameters that make the i_{on} value as close to 0 as possible should be adopted. In addition, when considering the design of coupled inductor, in order to prevent uneven distribution of core losses and uneven heating of the core, the magnetic flux distribution of each magnetic column should be as uniform as possible. Therefore, the parameters of coupled inductance can take $L = L_a$ = 21 μH, k = 0.5 as pointed out in Fig. 4(a). Consequently, the relationship between D and P_o can be obtained, as shown in Fig. 4(b). It can be seen that the proposed NIBBC can achieve the full load range of ZVS conditions for four switches within 500 W of power when D is changed from 0.4 to 0.6.

C. Derivation of inductor current expression

With the adding of the diode, the waveform of "i_{La}" will be forced to have positive bias due to the reverse current blocking capability. And this positive bias can be used to eliminate the DC bias in the main inductor i_L to help achieve ZVS. Due to the existence of the diode, the current cannot be negative, and the auxiliary inductor current i_{La} starts to rise from zero when S_2 and S_4 are turned on in a switching period. The current expression of main inductor can be derived according to the current of auxiliary inductor through magnetic field analysis with the initial condition: $i_{La}(t_0) = 0$. The details are as follows,

The expression of i_{La} in a switching period can be written as

$$i_{La}(t) = \begin{cases} \dfrac{V_o(L - k\sqrt{LL_a})}{LL_a(1-k^2)} \cdot t, & 0 \le t < (1-D)T_s \\ \dfrac{V_o T_s (1-D)(L - k\sqrt{LL_a})}{DLL_a(1-k^2)} - \dfrac{V_o(L - k\sqrt{LL_a})}{LL_a(1-k^2)} \cdot t, & (1-D)T_s \le t \le T_s \end{cases}. \tag{11}$$

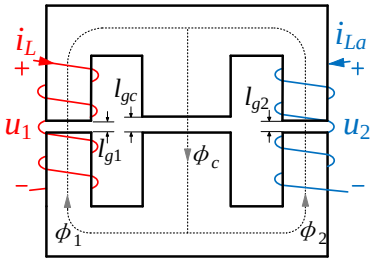

Fig. 5. The winding structure of coupled inductor.

The average currents of the two inductors and the average output current satisfy the following relationship

$$\overline{I_L} - \overline{I_{La}} = \frac{\overline{I_o}}{1-D} = \frac{P_o}{V_o(1-D)}. \tag{12}$$

The EE core is used for the coupled inductor, and the energy is transferred between the two windings through the magnetic flux as shown in Fig. 5, where ϕ_1 and ϕ_2 represent the magnetic flux passing through two outer legs respectively. R_1, R_2, and R_C represent the magnetic reluctance of the air gap l_{g1}, l_{g2} and l_{gc} respectively.

The relationship between the magnetic flux and the currents of the two inductors can be expressed as

$$\begin{bmatrix}\phi_1(t)\\ \phi_2(t)\end{bmatrix} = \begin{bmatrix}\frac{R_2+R_C}{\Delta R} & \frac{-R_C}{\Delta R}\\ \frac{-R_C}{\Delta R} & \frac{R_1+R_C}{\Delta R}\end{bmatrix}\begin{bmatrix}n_L i_L(t)\\ n_{La} i_{La}(t)\end{bmatrix} \tag{13}$$

where n_L and n_{La} are the turns of the two windings, and $\Delta R=R_1R_2+R_1R_C+R_2R_C$. The magnetic reluctance can be calculated as

$$\begin{bmatrix}R_1\\ R_C\\ R_2\end{bmatrix} = \mu_0\begin{bmatrix}\frac{l_{g1}}{A_{e1}} & \frac{l_{gC}}{A_{eC}} & \frac{l_{g2}}{A_{e2}}\end{bmatrix}^T \tag{14}$$

where μ_0 is the vacuum permeability, which is $4\pi\times10^{-10}$ H/mm, A_{e1}, A_{e2} and A_{eC} are the cross-sectional areas of the three magnetic columns respectively.

When the converter is in steady state operation, the difference between $\phi_1(t)$ and $\phi_2(t)$ can be expressed as

$$\phi_{1-2}(t) = \begin{cases}\int_0^{(1-D)T_s} V_o dt, & 0 \le t < (1-D)T_s\\ \int_{(1-D)T_s}^{T_s} \frac{1-D}{D} V_o dt, & (1-D)T_s \le t \le T_s.\end{cases} \tag{15}$$

Combining (11) - (15), the current $i_L(t)$ can be calculated as:

$$i_L(t) = \begin{cases}\frac{V_o T_s(1-D)(L+L_a-2k\sqrt{LL_a})}{2LL_a(1-k^2)} + \frac{P_o}{V_o(1-D)}\\ \quad -\frac{V_o(L_a-k\sqrt{LL_a})}{LL_a(1-k^2)}\cdot t, & 0 \le t < (1-D)T_s\\ \frac{V_o T_s(1-D)\left[DL-(2-D)L_a+2(1-D)k\sqrt{L\cdot L_a}\right]}{2DLL_a(1-k^2)} + \frac{P_o}{V_o(1-D)}\\ \quad +\frac{V_o(L_a-k\sqrt{LL_a})}{LL_a(1-k^2)}\cdot\frac{1-D}{D}t, & (1-D)T_s \le t \le T_s.\end{cases} \tag{16}$$

Fig. 6(a) shows the waveforms of i_L and i_{La} calculated according to (16) and (11). It can be seen that the calculated results are consistent with the simulated waveforms as shown in Fig. 6(b).

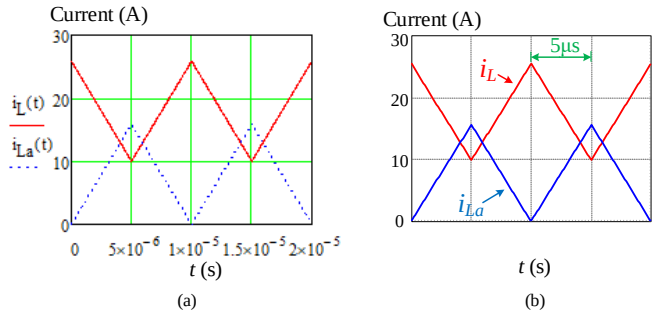

Fig. 6. The waveforms of inductor. (a) Calculated waveforms of i_L and i_{La}. (b) Simulated waveforms of i_L and i_{La}.

D. Comparison

Table I lists the comparison with the other five options. The schemes in [12] and [13] are suitable for low-power applications. Although the voltage level of the converter in the schemes [14]-[16] is similar to the proposed NIBBC, it uses more auxiliary devices such as auxiliary inductors and capacitors. The proposed NIBBC uses a coupled inductor to replace the single inductor of the traditional converter. Compared with other methods, it has the fewest auxiliary components. At the same time, the equivalent inductance can be changed, and the magnetic flux of the center column can be offset to reduce magnetic loss. By adding a diode, the peak

TABLE I Detailed parameter comparison

Topologies	In [12]	In [13]	In [14]	In [15]	In [16]	Proposed NIBBC
Number of switches	5	4	4	4	4	4
Number of inductors	2	3	5	4	3	2
Auxiliary switches	1	×	×	×	×	×
Auxiliary diodes	1	×	2	1	×	1
Auxiliary capacitors	×	2	×	1	4	×
Output voltage (V)	48	48	90	100	100	100
Output power (W)	75	60	322	400	220	500

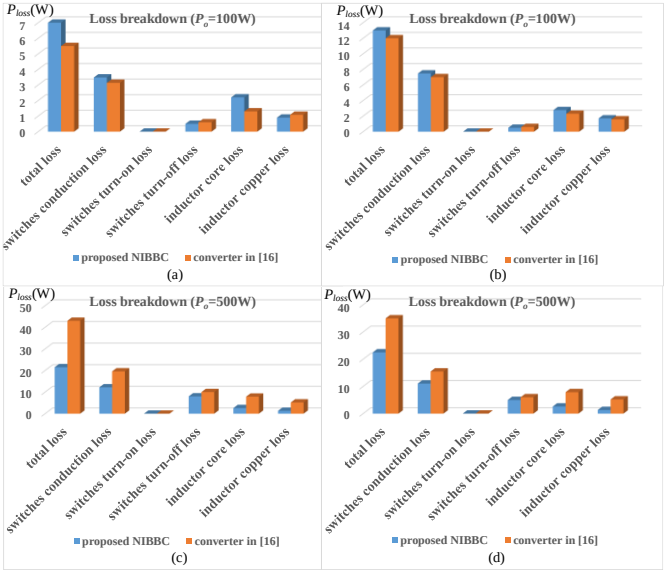

Fig. 7. Loss breakdown comparisons. (a) At light load (100W) when V_{in}=67V. (b) At light load (100W) when V_{in}=150V. (c) At heavy load (500W) when V_{in}=67V. (d) At heavy load (500W) when V_{in}=150V.

value of the auxiliary inductor current can be increased, thereby improving the ability to cancel the main inductor current to help achieve ZVS.

E. Loss breakdown comparisons

The loss breakdown comparisons of the proposed NIBBC and the converter in [16] under different loads and voltages are shown in Fig. 7. At light load (100W), Fig. 7(a) and Fig.7(b) show the loss breakdown under V_{in}=67V and V_{in}=150V respectively. When the converter works at light load (100W), the total loss of the proposed NIBBC is higher than that of the converter in [16], which is mainly caused by the larger current flowing through the switches, leading to larger conduction loss and larger core loss at light load. However, when the converter works at heavy load condition (500W), as Fig. 7(c) and Fig. 7(d) show, the total loss of the converter in [16] is higher than that of the proposed NIBBC, which is mainly caused by the increased conduction and core loss.

IV. EXPERIMENT RESULTS

A 500W prototype of the proposed NIBBC was built to verify the effectiveness of the solution, as shown in Fig. 8. For the MOSFETs, IRFB4332PBF was chosen. Due to the switch junction capacitance, the diode will have a temporary reverse voltage drop during the dead time. To ensure the safety, the SBR20U60CT with a rated voltage of 60V and a rated current of 20A was chosen. In addition, the parameters of method in [16] were listed to show a fair comparison, as shown in Table II.

Since ZVS achievement will become worse if the load increases, therefore, if the converter can realize ZVS under heavy load condition, ZVS can also be realized under light load condition. Fig. 9 shows the ZVS and current waveforms under half load condition when V_{in} = 150 V (D = 0.4). Before turning on the switch, the difference between the currents of the two inductors (i_L-i_{La}), which is the turn on current of switches, is negative, and the voltage across the switch has dropped to zero, so all the switches can be turned on at zero voltage as illustrated in the Figures. In the case of full load, although the turn on current of the switch is reduced, the ZVS condition still exists as shown in Fig. 10. Figs. 11 and 12 respectively show the realization of ZVS under full load condition and no-load condition of the converter when V_{in} = 67 V (D = 0.6). It can be concluded that the proposed NIBBC can achieve ZVS within full load range under different input voltages.

TABLE II Parameters of the prototype

Parameter	The Proposed Converter	Method in [16]
Input Voltage (V_{in})	67-150 V	
Output Voltage (V_o)	100 V	
Duty Cycle (D)	0.4-0.6	
Switching Frequency (f_s)	100 *k*Hz	
The MOSFETs (S_1-S_4)	IRFB4332PBF	
Main Inductance (L)	21 μH	21 μH
Auxiliary Inductance (L_a)	21 μH	$L_1 = L_2$ = 60 μH
Mutual Inductance (M)	10.5 μH	30 μH
The Diode	SBR20U60CT	—

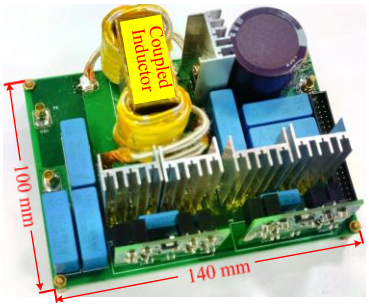

Fig. 8. Prototype of the proposed NIBBC.

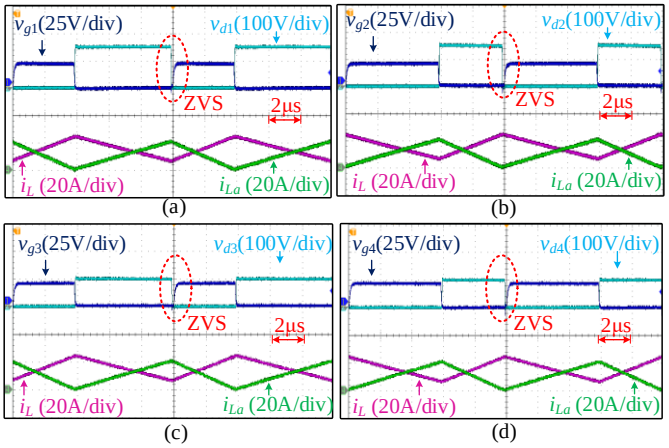

Fig. 9. ZVS waveforms of four switches under half load condition when D=0.4. (a) ZVS of S_1. (b) ZVS of S_2. (c) ZVS of S_3. (d) ZVS of S_4.

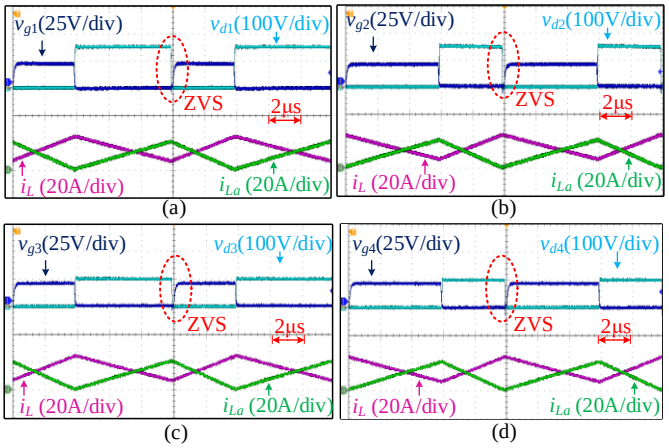

Fig. 10. ZVS waveforms of four switches under full load condition when D=0.4. (a) ZVS of S_1. (b) ZVS of S_2. (c) ZVS of S_3. (d) ZVS of S_4.

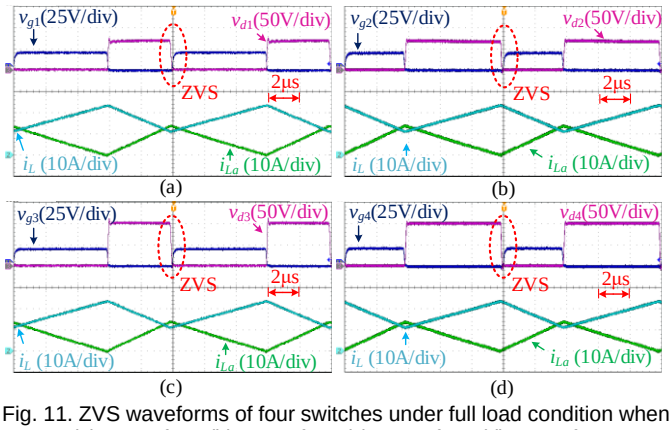

Fig. 11. ZVS waveforms of four switches under full load condition when D=0.6. (a) ZVS of S_1. (b) ZVS of S_2. (c) ZVS of S_3. (d) ZVS of S_4.

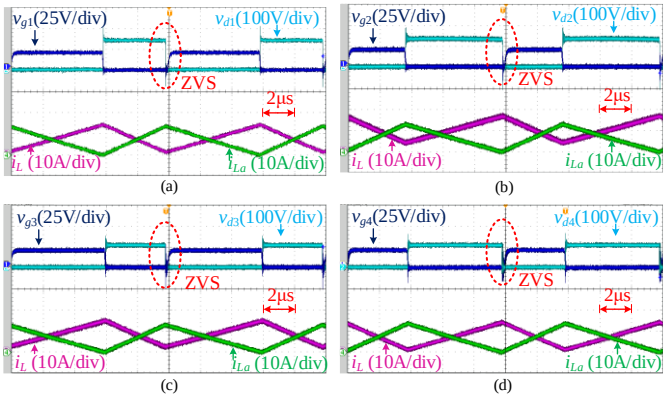

Fig. 12. ZVS waveforms of four switches under no-load condition when D=0.6. (a) ZVS of S_1. (b) ZVS of S_2. (c) ZVS of S_3. (d) ZVS of S_4.

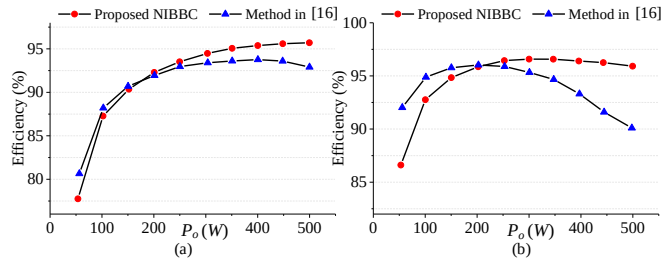

Fig. 13. Comparisons of measured efficiency. (a) D = 0.4. (b) D = 0.6.

Fig. 13 shows the measured efficiency curves of two converters: the NIBBC proposed in [16] and the proposed NIBBC in this paper. As the output power increases, the method in [16] has lower efficiency because there are more auxiliary components and higher related losses. When V_{in} = 67V (D = 0.6), the efficiency under heavy load condition decreases more obviously as shown in Fig. 13(b). The proposed NIBBC has a slightly lower efficiency under light load condition, but the efficiency is improved under heavy load condition and the maximum efficiency is 96%.

V. Conclusion

In this paper, a new NIBBC is obtained by using the coupled inductor as the main inductor, and the auxiliary current generated by the magnetic coupling effect is used to obtain the soft switching conditions of all switches. The new NIBBC has fewer auxiliary devices while achieving higher conversion efficiency. This paper presents the topology analysis and mathematical model of the new NIBBC, and derives the conditions for realizing full-range soft switching. Finally, an experimental prototype was built to verify the effectiveness of the proposed converter and design.

References

[1] X. Weng et al., "Comprehensive comparison and analysis of non-inverting buck boost and conventional buck boost converters," in *The Journal of Engineering*, vol. 2019, no. 16, pp. 3030-3034, 3 2019.

[2] Y. Babazadeh, E. Babaei and M. Sabahi, "A new non-isolated buck-boost converter with high voltage gain and positive output voltage for renewable energy applications," *2019 10th International Power Electronics, Drive Systems and Technologies Conference (PEDSTC)*, Shiraz, Iran, 2019, pp. 201-206.

[3] H. Liu, K. Qu, Y. Wang, W. Jiang, J. Zhao and J. Xu, "A wide output non-isolated boost-buck converter," *2019 4th International Conference on Intelligent Green Building and Smart Grid (IGBSG)*, Hubei, Yi-chang, China, 2019, pp. 508-511.

[4] A. Rodriguez, A. Barrado, C. Calderon, A. Lazaro and P. Zumel, "Magnetically coupled buck-boost bidirectional DC-DC converter," in *IEEE Transactions on Industrial Electronics*, doi: 10.1109/TIE.2020.3020011.

[5] J. Han, F. Li, J. Zheng, Z. Chen, L. Bu and L. Song, "Low switching loss non-isolated DC-DC buck-boost converter with ZCS characteristics," *2019 14th IEEE Conference on Industrial Electronics and Applications (ICIEA)*, Xi'an, China, 2019, pp. 1322-1326.

[6] F. Li, R. Hao, H. Lei, X. You, C. Ke and J. Wang, "Non-inverting three-level buck-boost converter for wide voltage range application," *2018 IEEE Energy Conversion Congress and Exposition (ECCE)*, Portland, OR, USA, 2018, pp. 4870-4875.

[7] V. Siddhartha and Y. V. Hote, "Non-inverting buck-boost derived hybrid converter," *2016 International Conference on Emerging Trends in Electrical Electronics & Sustainable Energy Systems (ICETEESES)*, Sultanpur, 2016, pp. 234-240.

[8] J. Moon et al., "60-V non-inverting four-mode buck-boost converter with bootstrap sharing for non-switching power transistors," in *IEEE Access*, vol. 8, pp. 208221-208231, 2020.

[9] J. Yu, M. Liu, D. Song, J. Yang and M. Su, "A soft-switching control for cascaded buck-boost converters without zero-crossing detection," in *IEEE Access*, vol. 7, pp. 32522-32536, 2019.

[10] C. Tsai, Y. Tsai and H. Liu, "A stable mode-transition technique for a digitally controlled non-inverting buck–boost DC–DC converter," in *IEEE Transactions on Industrial Electronics*, vol. 62, no. 1, pp. 475-483, Jan. 2015.

[11] A. Borzooy, S. A. Khajehoddin, M. Karimi Ghartemani and M. Ebrahimi, "An alternative control approach to achieve fast load transient responses in DC-DC converters," in *IEEE Transactions on Industrial Electronics*, doi: 10.1109/TIE.2020.3040675.

[12] L. Cong, J. Liu and H. Lee, "A high-efficiency low-profile zero-voltage transition synchronous non-inverting buck-boost converter with auxiliary-component sharing," in *IEEE Transactions on Circuits and Systems I*: Regular Papers, vol. 66, no. 1, pp. 438-449, Jan. 2019.

[13] J. Xue and H. Lee, "A 2-MHz 60-W zero-voltage-switching synchronous noninverting buck–boost converter with reduced component values," in *IEEE Transactions on Circuits and Systems II*: Express Briefs, vol. 62, no. 7, pp. 716-720, July 2015.

[14] X. Cheng, Y. Zhang and C. Yin, "A zero voltage switching topology for non-inverting buck–boost converter," in *IEEE Transactions on Circuits and Systems II*: Express Briefs, vol. 66, no. 9, pp. 1557-1561, Sept. 2019.

[15] Y. Zhang, X. Cheng and C. Yin, "A soft-switching synchronous rectification non-inverting buck-boost converter with a new auxiliary circuit," in *IEEE Transactions on Industrial Electronics*, doi: 10.1109/TIE.2020.3009574.

[16] Y. Zhang, X. Cheng and C. Yin, "A soft-switching non-inverting buck–boost converter with efficiency and performance improvement," in *IEEE Transactions on Power Electronics*, vol. 34, no. 12, pp. 11526-11530, Dec. 2019.

[17] S. Sharifi, M. Jabbari and H. Farzanehfard, "A New Family of Single-Switch ZVS Resonant Converters," in IEEE Transactions on Industrial Electronics, vol. 64, no. 6, pp. 4539-4548, June 2017.

[18] D. O. Neacșu, M. N. Cirstea and D. Butnicu, "Comparative Reliability Analysis for Resonant Converter Operation Under Component Ageing," in IEEE Journal of Emerging and Selected Topics in Industrial Electronics, vol. 2, no. 2, pp. 142-154, April 2021.

[19] Y. Zhang et al., "Low-frequency ripple-shaping controller for operation of non-inverting buck-boost converters near step-up step-down boundary," 2018 IEEE Applied Power Electronics Conference and Exposition (APEC), 2018, pp. 292-297.

[20] Y. Zhang et al., "Multilevel Non-Inverting Buck-Boost Converter with Low-Frequency Ripple-Shaping Based Controller for Operating in Step-down/Step-up Transition Region," 2018 IEEE 19th Workshop on Control and Modeling for Power Electronics (COMPEL), 2018, pp. 1-7.